Journal of Computational Physics **169,** 193–214 (2001)
doi:10.1006/jcph.2001.6722, available online at http://www.idealibrary.com on IDEAL®

Underresolved Simulations of Heat Baths

B. Cano*,[1] and A. M. Stuart†

*Departamento de Matemática Aplicada y Computación, Facultad de Ciencias, Universidad de Valladolid, Valladolid, Spain; and †Mathematics Institute, Warwick University, Coventry CV4 7AL, United Kingdom

Received February 24, 2000; revised October 30, 2000

Some recent numerical and theoretical studies indicate that it is possible to accurately simulate the macroscopic motion of a particle in a heat bath, comprising coupled oscillators, without accurately resolving the fast frequencies in the heat bath itself. Here we study this issue further by performing numerical experiments on a wide variety of mechanical heat bath models, all generalizations of the Ford–Kac oscillator model. The results indicate that the nature of the particle-bath damping in the macroscopic limit crucially affects the ability of underresolved simulations to correctly predict macroscopic behaviour. In particular, problems for which the damping is local in time pose more severe problems for approximation. The root cause is that local damping typically arises from the degeneration of a memory kernel to a delta singularity in the macroscopic limit. The approximation of such singularities is a more delicate issue than the approximation of smoother memory kernels.

Key Words: mechanical heat baths; underresolved simulations; coupled oscillators; stiff oscillatory systems; symplectic integration.

1. INTRODUCTION

There are many problems in which an initial value problem involving a large number of variables may be partitioned into the form

$$\begin{aligned} \frac{dx}{dt} &= a(x, y), \quad x(0) = x_0, \\ \frac{dy}{dt} &= b(x, y), \quad y(0) = y_0, \end{aligned} \tag{1.1}$$

where only the variable x is of intrinsic interest; y is of interest only in as much as its evolution affects x. If $x \in \mathbb{R}^d$ and $y \in \mathbb{R}^D$ with $D \gg d$, it is desirable to find economical

[1] Supported by JCL VA36/98 and DGICYT PB95-705.

0021-9991/01 $35.00

integration schemes which expend only minimal effort to calculate accurately the influence of y on x without resolving all the details of y. It is not possible to study such economical schemes in a completely general way, but progress can be made if further structure is assumed on the problem.

The structure which we choose to work with occurs when the variable y represents a generalized heat bath and the variables (x_0, y_0) are distributed according to a measure whose parameters encapsulate known properties of the bath. For these and other related problems, one approach developed by Chorin *et al*. [2, 3] is to find an equation for $X(t) = \mathbb{E}x(t)$ where expectation is with respect to a measure ν on (x_0, y_0). This reduces the dimension of the system from $D + d$ to d, and hence reduces the complexity of an integration scheme. The methodology has been used with some success, although theoretical justification is in its early stages; study of some simple heat bath models, like those studied here, appears to provide further theoretical understanding [9] as does the work of Hald [7].

The approach we study here is different. The full system (1.1) *is* integrated but a time-step is chosen which is large relative to time-scales in the heat bath represented by y—formally y will be computed inaccurately but it may still be possible to compute its effect on x satisfactorily. We reemphasize that the motivation for such integration schemes is to reduce computational cost by choosing a time-step which is as large as possible, given the objective of computing x accurately. *The main goal of this work is to study phenomena associated with underresolved simulation; we are not advocating specific methods*. Hence our numerical simulations are, for the most part, performed within a single parametrized family of first-order methods; the family includes the symplectic Euler method. In Section 6 we illustrate the implications of our study for commonly used methods such as velocity Verlet and multiple time-scale methods.

To address the accuracy questions for x, the general framework we study is Hamiltonians of the form

$$H = \frac{1}{2}|p|^2 + V(|q|) + \sum_{j=1}^{N} \left\{ \frac{1}{2}\frac{|v_j|^2}{m_j} + F_j(u_j, q) \right\}. \tag{1.2}$$

Here $p, q, u_j, v_j \in \mathbb{R}^n$ and $|\cdot|$ denotes the Euclidean norm on $\mathbb{R}^n$. The variables are paired canonically as $x = (p, q)$, $y = \{(v_j, u_j)\}_{j=1}^N$. In [12] the case where

$$n = 1, \quad m_j = \frac{1}{j^2}, \quad F_j(w, z) = \frac{1}{2}(w - z)^2$$

is studied. In this case, for N large and a certain Gaussian measure ν on the initial data for $\{(v_j, u_j)\}_{j=1}^N$, q is provably close to the solution Q of a stochastic differential equation (SDE) in $\mathbb{R}^2$. It is natural to ask whether numerical simulations can accurately predict this large N behaviour for q without accurately resolving all the y variables. Since

$$\ddot{u}_j + j^2(u_j - q) = 0,$$

the fastest natural frequency in y is $\mathcal{O}(N)$ and a candidate inaccurate (and economical) simulation is one for which $N\Delta t$ is fixed so that y is not fully resolved; in any case, fixing $N\Delta t$ is natural from the stability viewpoint for explicit schemes.[2] Numerical experiments

[2] A restriction on $\xi = N\Delta t$ required for convergence may be viewed as a CFL-like condition, analogous to those arising in approximation of PDEs; see [10].

performed in the regime

$$N\Delta t = \xi, \quad \Delta t \to 0, \quad N \to \infty \tag{1.3}$$

show [12] that certain numerical methods accurately approximate the SDE limit for q while others do not. Those methods which fail to capture the limit correctly appear to compute a different limit satisfying a modified SDE. Analysis which goes some way toward justifying the experiments in [12] may be found in [1].

A natural criticism of the work in [1, 12] is that the model problems are too simple—if the limit SDE is actually known explicitly then there is no need to solve the large Hamiltonian system. The purpose of this paper is to show that results similar to those in [12] may be observed in more complex situations where a limiting stochastic process for q is not necessarily known to exist, or does not have the simple form of an SDE. To this end, we study numerical methods for (1.1) under (1.3) in the four cases

$$n = 1, \quad m_j = \frac{1}{j^2}, \quad F_j(w,z) = \frac{(w-z)^4}{4}; \tag{1.4}$$

$$n = 3, \quad m_j = \frac{1}{j^2}, \quad F_j(w,z) = \frac{|w-z|^2}{2}; \tag{1.5}$$

$$n = 1, \quad m_j = \frac{1}{j^2}, \quad F_j(w,z) = k_j \frac{(w-z)^2}{2}, \tag{1.6}$$

where k_j is a random variable chosen so that the natural frequencies of the springs are uniform random variables in the interval $[0, N]$; and

$$n = 1, \quad m_j = 1, \quad F_j(w,z) = \frac{1}{2} j^2 w^2 - w f(z). \tag{1.7}$$

We present the results of numerical experiments for (1.4), (1.5), (1.6), and (1.7) in Sections 2, 3, 4, and 5, respectively. The results show that the observations made in [12] and [1] do carry over to more complex problems.

The first-order form of equations derived from (1.2), and which we want to integrate, is

$$\begin{aligned} \dot{p} &= -V'(|q|)\frac{q}{|q|} - \sum_{j=1}^{N} \frac{\partial F_j}{\partial q}(u_j, q), \\ \dot{q} &= p, \\ \dot{v}_j &= -\frac{\partial F_j}{\partial u_j}(u_j, q), \\ \dot{u}_j &= \frac{v_j}{m_j}. \end{aligned} \tag{1.8}$$

Here, and in the remainder of the paper, $\frac{\partial F_j}{\partial u_j}$ denotes the gradient of F_j with respect to u_j and $\frac{\partial F_j}{\partial q}$ denotes the gradient of F_j with respect to q. Formally $u_j(t)$ can be written, abusing notation, as

$$u_j(t) = \mathcal{H}_j(t) := \mathcal{H}_j(\{q(s)\}_{0 \le s \le t}, u_j(0), v_j(0))$$

and so we obtain the history-dependent equations

$$\ddot{q} + V'(|q|)\frac{q}{|q|} + \sum_{j=1}^{N} \frac{\partial F_j}{\partial q}(\mathcal{H}_j, q) = 0. \tag{1.9}$$

In the absence of the third term, we have a simple mechanical system describing frictionless motion in a potential V. The third term represents coupling to the heat bath. By choosing $u_j(0), v_j(0)$ at random, $\mathcal{F}_j$ is rendered random and so we have a random history-dependent functional equation for q. We refer to the behaviour of this equation for $N \to \infty$ as the *macroscopic limit*. Our objective is to accurately reproduce solutions of (1.9) in the macroscopic limit, by solving the system (1.8) numerically, but without necessarily resolving u_j and v_j accurately. As we shall see, the extent to which this is possible depends heavily on the nature of the particle–bath coupling in the limit $N \to \infty$.

For simplicity we detail here the three numerical methods ESM, ENSM1, and ENSM2, which are a principal object of study throughout the paper. The symplectic Euler method, which is an explicit symplectic method and is denoted by ESM, is defined by

$$\begin{aligned}
p^{n+1} &= p^n - \Delta t V'(|q^n|)\frac{q^n}{|q^n|} - \Delta t \sum_{j=1}^{N} \frac{\partial F_j}{\partial q}\big(U_j^n, q^n\big),\\
q^{n+1} &= q^n + \Delta t p^{n+1},\\
V_j^{n+1} &= V_j^n - \Delta t \frac{\partial F_j}{\partial u_j}\big(U_j^n, q^n\big),\\
U_j^{n+1} &= U_j^n + \Delta t \frac{V_j^{n+1}}{m_j}.
\end{aligned} \tag{1.10}$$

We will also consider the explicit nonsymplectic methods

$$\begin{aligned}
p^{n+1} &= p^n - \Delta t V'(|q^n|)\frac{q^n}{|q^n|} - \Delta t \sum_{j=1}^{N} \frac{\partial F_j}{\partial q}\big(U_j^n, q^n\big),\\
q^{n+1} &= q^n + \Delta t p^n,\\
V_j^{n+1} &= V_j^n - \Delta t \frac{\partial F_j}{\partial u_j}\big(U_j^n, q^n\big),\\
U_j^{n+1} &= U_j^n + \Delta t \frac{V_j^{n+1}}{m_j},
\end{aligned} \tag{1.11}$$

denoted here by ENSM1, and

$$\begin{aligned}
p^{n+1} &= p^n - \Delta t V'(|q^n|)\frac{q^n}{|q^n|} - \Delta t \sum_{j=1}^{N} \frac{\partial F_j}{\partial q}\big(U_j^{n+1}, q^n\big),\\
q^{n+1} &= q^n + \Delta t p^{n+1},\\
V_j^{n+1} &= V_j^n - \Delta t \frac{\partial F_j}{\partial u_j}\big(U_j^n, q^n\big),\\
U_j^{n+1} &= U_j^n + \frac{\Delta t}{m_j} V_j^{n+1},
\end{aligned} \tag{1.12}$$

denoted here by ENSM2.

All three of these methods are particular cases of the general scheme

$$\begin{aligned} p^{n+1} &= p^n - \Delta t V'(|q^n|)\frac{q^n}{|q^n|} - \Delta t \sum_{j=1}^{N} \frac{\partial F_j}{\partial q}\left(U_j^{n+\theta}, q^{n+\phi}\right), \\ q^{n+1} &= q^n + \Delta t p^{n+\sigma_1}, \\ V_j^{n+1} &= V_j^n - \Delta t \frac{\partial F_j}{\partial u_j}\left(U_j^{n+1-\alpha}, q^{n+1-\alpha}\right), \\ U_j^{n+1} &= U_j^n + \frac{\Delta t}{m_j}\left(V_j^n - \alpha \Delta t \frac{\partial F_j}{\partial u_j}\left(U_j^n, q^n\right)\right). \end{aligned} \tag{1.13}$$

We emphasize that we are not advocating use of this general scheme; it is only of practical interest in the ESM case. However, our results may be of interest since they indicate the issues that arise, and the caution that must be exercised, when integrating stiff oscillatory systems in the underresolved limit. In Section 6 we discuss related issues for methods commonly used in the molecular dynamics literature, such as velocity Verlet and multiple time-scale methods.

The parameters $\alpha, \theta, \phi,$ and σ_1 have the following values for the three methods detailed above:

- **ESM:** $\alpha = 1, \theta = 0, \phi = 0, \sigma_1 = 1$;
- **ENSM1:** $\alpha = 1, \theta = 0, \phi = 0, \sigma_1 = 0$;
- **ENSM2:** $\alpha = 1, \theta = 1, \phi = 0, \sigma_1 = 1$.

We note that none of the methods in (1.13) are symmetric (i.e., time-reversible). Moreover, among them, only ESM and the one corresponding to $\alpha = 0, \theta = 1, \phi = 1, \sigma_1 = 0$, are symplectic. All the others are not. (This can be proved in a straightforward way from the definitions of symmetry and symplecticity). Our numerical studies in this paper, and some analysis in [12], indicate that the conditions

$$\alpha + \theta = 1, \quad \theta = \phi, \tag{1.14}$$

are both necessary and sufficient for accurate resolution of (p, q) in underresolved simulations of certain heat bath models, on finite time intervals. Both ESM and ENSM1 satisfy (1.14) and thus neither symmetry nor symplecticity appears necessary for accurate resolution of the macroscopic variables (p, q).[3]

Although our purpose in this paper is to analyse and understand certain phenomena associated with underresolved integration of heat baths, and not to propose the best methods to do so, in Section 6 we extend our study of the integrators (1.13) to others widely used in molecular dynamics problems, such as velocity Verlet or multiple time-scale integrators [13, 14]. These methods are symplectic and symmetric and all perform well in terms of reproducing the macroscopic limit. However, we show that in terms of error per unit cost, with error measured in the macroscopic variables only, the multiple time-scale methods are not competitive.

The overview of this paper is as follows: we have conducted numerical experiments which investigate the numerical simulation of mechanical heat baths in the form (1.8); these heatbaths generalize the Ford–Kac model described in [4, 15]. The methods are applied

[3] It is likely that this conclusion might change radically for long-time simulations, but these are not the object of study in this paper.

under a CFL-like condition (1.3) which precludes accurate resolution of fast scales. The question of interest is whether slowly varying quantities, governed by (1.9), are accurately represented. Our aim is to further the analysis and experiments conducted in [1] and [12] by studying a wider variety of problems.

Heuristically the effect of the heat bath coupling in (1.9) for large N may be broken into two components—a damping term representing loss of energy from the particle of interest q to the heat bath, and a stochastic force, representing gain of energy to q from the bath, with stochasticity introduced through the initial data. The numerical results we give seem to indicate that, if the heat bath coupling gives rise to **local** (in time) damping, then the observations of [1, 12] extend to more complex situations (see Sections 2, 3, and 4). That is, certain methods, such as ESM and ENSM1, compute the correct macroscopic limit for q, while others, such as ENSM2, fail to do so. If, however, the damping is **nonlocal** in time, as in the Habib–Kandrup model of Section 5, then this distinction between methods disappears and all of the methods studied appear to compute the correct macroscopic limit.

2. NONLINEAR SPRING COUPLING

Here we consider (1.2) under (1.4) which yields the equations

$$\begin{aligned} \ddot{q} + V'(q) &= \sum_{j=1}^{N} (u_j - q)^3, \\ \ddot{u}_j + j^2(u_j - q)^3 &= 0. \end{aligned} \tag{2.1}$$

We consider $V(z) = \frac{1}{4}(1 - z^2)^2$ and initial data

$$q(0) = 1.5, \quad \dot{q}(0) = 0, \quad u_j(0) = \alpha_j, \quad \dot{u}_j(0) = 0, \tag{2.2}$$

where α_j are chosen i.i.d. from a random variable with density proportional to $e^{-(x^4/4)}$. Note that this is the macrocanonical invariant density for u_j if $q \equiv 0$, that is if the heat bath is uncoupled; it is hence a natural choice for initial data. No explicit stochastic process characterizing q for large N is known here. However the solutions appear to approach a limit as $N \to \infty$ and accurate solutions for q and $p = \dot{q}$ with $N = 32,000$ and $N\Delta t = 10^{-3}$ (well-resolved) are shown in Fig. 1. (Taking $N = 64{,}000$ and $N\Delta t = 0.5 \times 10^{-3}$ gives essentially the same result, substantiating our claim that there is a macroscopic limit

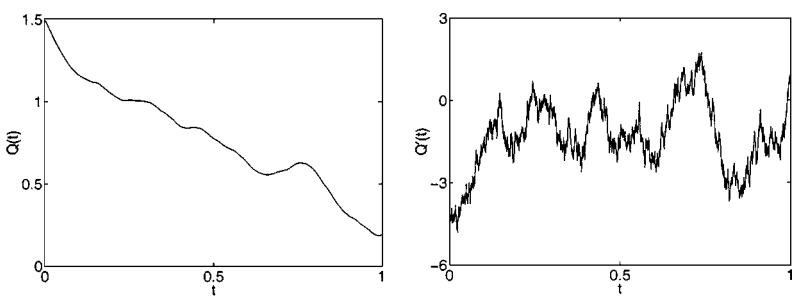

FIG. 1. Exact position and velocity of the distinguished particle in the problem with nonlinear spring coupling.

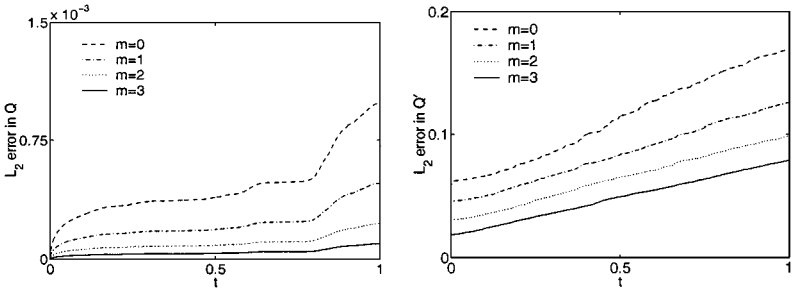

FIG. 2. $L2$-error curves for the position and velocity of the distinguished particle when integrating with ESM.

$N \to \infty$.) Hereafter we refer to this as the "exact" solution and denote it by Q, tacitly assuming that it represents the solution of some limiting stochastic problem found from (1.9) in the macroscopic limit. We now approximate (2.1) by the three methods (1.10), (1.11), and (1.12) under (1.3) with $\xi = 0.1$. Figures 2 and 3 show that the methods ESM and ENSM1 approximate the "exact" solution for $\dot{q}$ with increasing accuracy as m increases, where $N = 1000 \times 2^m$; similar convergence is observed for the position q, although the errors are smaller. (Notice that we are measuring the error in the L_2-norm, so that this error increases with time by definition.) Similar results are observed for the L_∞ error in physically interesting quantities such as position and/or velocity auto-correlations: the methods ESM and ENSM1 converge. See Section 6.

For all our numerical experiments we perform best fits to the data to estimate rates of convergence; here, and in all other cases, these are done for single realizations with respect to the probability measure on the data. A least squares fit of the log–log plot of L_2—the errors for the considered initial data—shows that the rate of convergence for these errors is $(\Delta t)^e$, where $e = 1.1147$ for ESM and q; $e = 1.0997$ for ENSM1 and q; $e = 0.3659$ for ESM and $\dot{q}$; and $e = 0.3752$ for ENSM1 and $\dot{q}$. However, for the ENSM2 no such convergence is observed–Fig. 4 compares the position Q as calculated exactly and under (1.3) with $N = 8000$, $\xi = 0.1$.[4]

The observations about the relative merits of these schemes correspond exactly to those made in [12] for which the spring coupling is linear: in that case the limiting exact solution is known to be the solution of an explicit SDE, found from (1.9) as $N \to \infty$, and only ESM and ENSM1 compute this limit correctly under (1.3). Our experiments show that insight obtained for the linear spring coupling sheds light on the efficacy of numerical methods with a stronger nonlinear coupling for which an explicit macroscopic limit is not known.

3. LINEAR SPRINGS

Here we consider (1.2) under (1.5) giving

$$\begin{aligned} \ddot{q} + V'(|q|)\frac{q}{|q|} &= \sum_{j=1}^{N}(u_j - q), \quad q(0) = q_0, \quad \dot{q}(0) = p_0 \\ \ddot{u}_j + j^2(u_j - q) &= 0, \quad u_j(0) = \alpha_j, \quad \dot{u}_j(0) = 0. \end{aligned} \tag{3.1}$$

[4] It is worth mentioning at this point that the total energy of the system is not a useful diagnostic in this case; the relative energy errors for ESM and ENSM2 are indistinguishable—see Section 6.

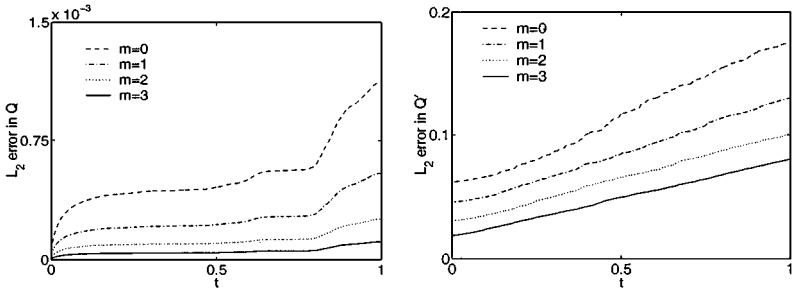

FIG. 3. *L*2-error curves for the position and velocity of the distinguished particle when integrating with ENSM1.

Again we take $V(z) = \frac{1}{4}(1-z^2)^2$ and the initial data (2.2) where now $q_0,\ p_0,\ \alpha_j \in \mathbb{R}^3$ and each component α_j is distributed according to a density proportional to $e^{-(x^4/4)}$. Calculation as in [12] shows that u_j may be eliminated to give

$$\ddot{q} + V'(|q|)\frac{q}{|q|} + \int_0^t K_N(t-s)\dot{q}(s)ds = -K_N(t)q(0) + Z_N(t),$$
$$q(0) = q_0, \quad \dot{q}(0) = p_0.$$

Here

$$K_N(t) = \sum_{j=1}^{N} \cos(jt)$$

and

$$Z_N(t) = \sum_{j=1}^{N} \alpha_j \cos(jt).$$

Because the α_j are not Gaussian the limiting behaviour of $Z_N(t)$ for large N is no longer a Gaussian white noise process as it is in [12]. However, using results in [8] it may be proved

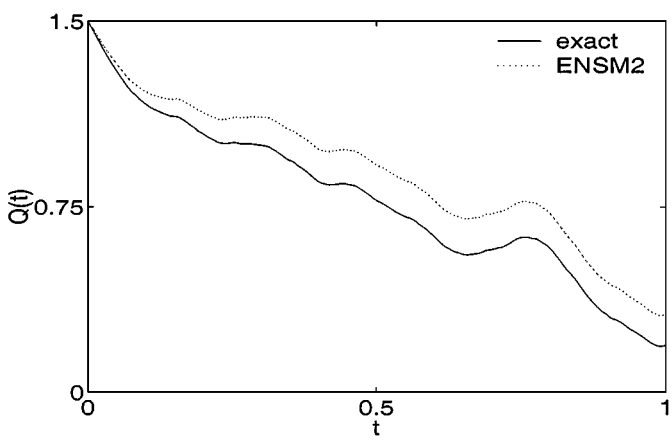

FIG. 4. Position of the distinguished particle when integrated accurately ("exact") and when integrated with ENSM2 ($N = 8000$, $N\Delta t = 0:1$).

that, almost surely,

$$\int_0^t Z_N(s)\,ds \to W(t)$$

where $W(t)$ is continuous. Note also that $K_N(t)$ has a delta-like singularity for large N, $(K_N(t) \approx \pi\delta(t) - \frac{1}{2})$ rendering the damping term

$$\int_0^t K_N(t-s)\dot{q}(s)\,ds$$

local in time.

We believe that analysis similar to that in [12] would enable proof that, for large N, q is close to Q, solving the (formal) SDE

$$\begin{aligned} \ddot{Q} + \frac{\pi}{2}\dot{Q} + V'(|Q|)\frac{Q}{|Q|} - \frac{1}{2}Q &= \dot{W}, \\ Q(0) = q_0, \quad \dot{Q}(0) &= p_0 - \frac{\pi}{2}q_0. \end{aligned} \tag{3.2}$$

A rigorous interpretation of this equation would require formulation as an integral equation. Figure 5 shows the Euclidean norm of the "exact" solution of (3.1) for $N\Delta t = 10^{-3}$ and $N = 32,000$, taking $q_0 = (1.5, 1.5, 1.5)^T$ and $p_0 = (0, 0, 0)^T$. Thus we believe that this will be a good approximation to a solution Q of (3.2) with a particular choice of noise related to the specific choice of α_j.

Based on the analogy with the work in [12] we conjecture that the numerical method (1.13), if integrated in the regime (1.3), will approximate not necessarily (3.2), but rather the possibly shifted limit

$$\begin{aligned} \ddot{Q} + \left\{\frac{\pi}{2} + \xi(\phi - \theta)\right\}\dot{Q} + V'(|Q|)\frac{Q}{|Q|} - \frac{1}{2}Q &= \dot{W}, \\ Q(0) = q_0, \quad \dot{Q}(0) &= p_0 - q_0\left\{\frac{\pi}{2} + \xi(1 - \alpha - \theta)\right\}. \end{aligned} \tag{3.3}$$

Note that θ, α, and ϕ are parameters of the method (1.13). Thus we are conjecturing that the computed macroscopic behaviour will depend upon the method used, a highly unsatisfactory situation. This conjecture is borne out in experiments. Figure 6 shows the errors in $\dot{q}$

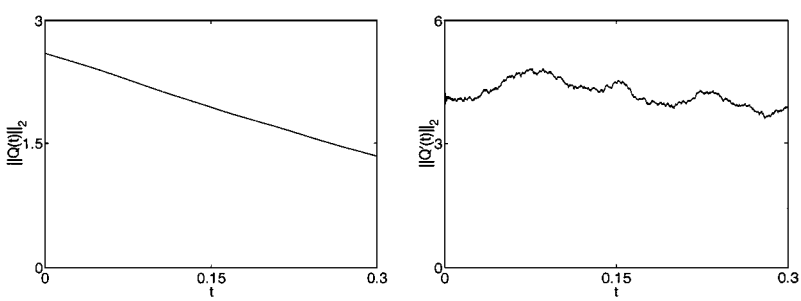

FIG. 5. Euclidean norm of the "exact" position and velocity of the distinguished particle in the 3*D*–linear problem.

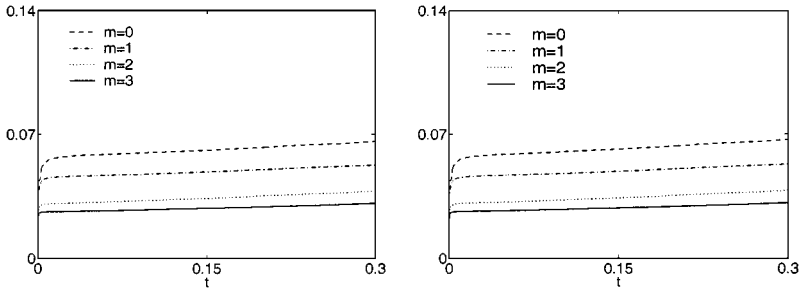

FIG. 6. $L2$-error curves for the velocity of the distinghished particle when integrating with ESM and ENSM1, respectively.

(compared with the "exact" solution) under (1.3) with $\xi = 1$ and $N = 1000 \times 2^m$, $m = 0, 1, 2, 3$ for both ESM and ENSM1. Since $\theta = \phi$ and $\theta + \alpha = 1$ for both these methods, Eqs. (3.2) and (3.3) are identical and we see convergence to the correct macroscopic limit, namely the solution of (3.2). Here the exponents in the rates of convergence can be calculated to be 0.3733 for ESM and 0.3786 for ENSM1 measured in $\dot{q}$. The rates of convergence in the position q for both methods are 1.0346 and 1.0663, respectively. Figure 7 compares the euclidean norm of $\dot{q}$ for the "exact" solution and as computed by the ENSM2, for which $\theta - \phi = 1, \theta + \alpha = 2$. As conjectured the correct limit is not calculated. However, if the error is calculated based on a comparison with solution of Eq. (3.3), then convergence is observed—see Fig. 8, again $N = 1000 \times 2^m$, $m = 0, 1, 2, 3$, and $\xi = 1$ in (1.3).

Thus, once again, we have a correspondence with our observations in [1, 12]; note that here our analysis is not as complete as in [12] because the noise is not Gaussian white. It is hence interesting that insight gained from [12] applies in this more general situation.

4. 1D RANDOM FREQUENCIES PROBLEM

In this section, we consider problem (1.2) under (1.6). The precise choice of the parameters is made as follows. Define $k_j > 0$ by $\omega_j^2 = j^2 k_j$ and choose ω_j to be the jth order statistic

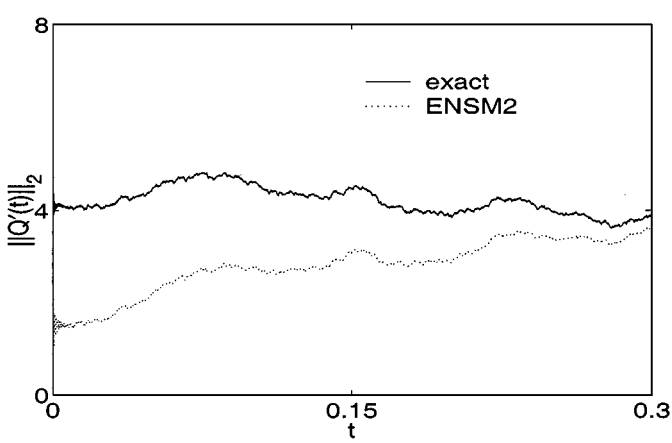

FIG. 7. Euclidean norm of the velocity of the distinghished particle when integrating accurately ("exact") and when integrating with ENSM2 ($N = 8000$, $N\Delta t = 1$).

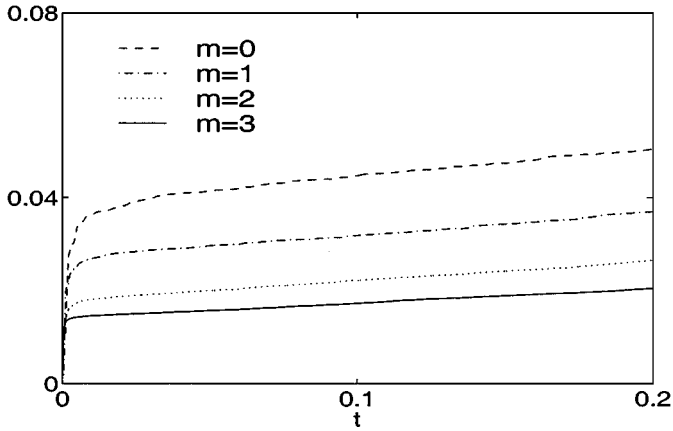

FIG. 8. *L*2-error curves for the velocity of the distinguished particle when integrating with ENSM2 and taking as exact solution (3.3).

in a random sample of M numbers from $\mathcal{U}[0, M]$.[5] The integer M is chosen larger than or equal to any N used in subsequent numerical experiments. This defines the $\{\omega_j\}$ and hence the $\{k_j\}$. This set of $\{\omega_j, k_j\}$ is chosen at random once and then the same set is used in all subsequent numerical experiments.

We have considered $M = 32{,}000$ and have used the first N of the $\{\omega_j, k_j\}$ thus generated as the frequencies of the linear springs in the following problem, which is (1.8) under (1.6):

$$\begin{aligned} \ddot{q} &= -V'(q) + \sum_{j=1}^{N} k_j(u_j - q), \\ \ddot{u}_j &= -\omega_j^2(u_j - q), \quad j = 1, \ldots, N, \\ q(0) &= 1.5, \quad \dot{q}(0) = 0, \quad u_j(0) = \alpha_j, \quad \dot{u}_j(0) = 0. \end{aligned} \tag{4.1}$$

The $\{\alpha_j\}_{j=1}^N$ are chosen as i.i.d. samples from a Gaussian distribution with mean 0 and variance 1. Eliminating u_j in (1.8) we obtain

$$\ddot{q} + V'(q) + \int_0^t K_N(t-s)\dot{q}(s)ds = -K_N(t)q(0) + Z_N(t), \tag{4.2}$$

where

$$K_N(t) := \sum_{j=1}^{N} k_j \cos(\omega_j t)$$

and

$$Z_N(t) := \sum_{j=1}^{N} k_j[\alpha_j \cos(\omega_j t)].$$

[5] The notation $\mathcal{U}[a, b]$ denotes the uniform distribution on $[a, b]$. The order statistics are ordered with smallest first, largest last.

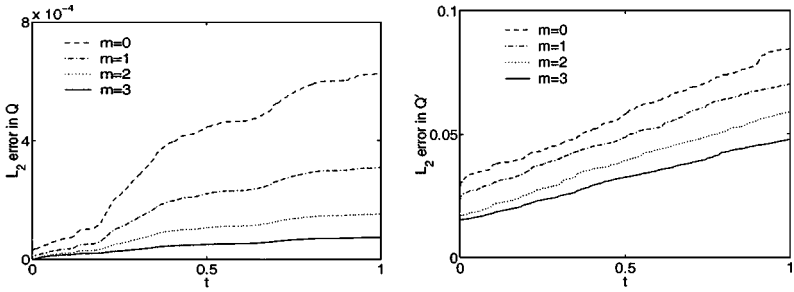

FIG. 9. *L*2-error curves for the position and velocity of the distinguished particle when integrating the linear springs problem with random frequencies with ESM.

This is a specific instance of (1.9). Although we have not proved it, we believe that this equation gives rise to a limiting SDE governing the motion of q for $N \to \infty$ and we proceed on the assumption that this is so.

We have approximated this macroscopic limit of the problem by solving (4.1) with $N = 32{,}000$ and $N \times \Delta t = 10^{-3}$—the "exact" solution. We have then compared this with the numerical solutions obtained from (1.10), (1.11), and (1.12) under (1.3) with $\xi = 1$, taking $N = 1{,}000 \times 2^m$ with $m = 0, 1, 2, 3$.

The results are very similar to those obtained in the previous sections. There is convergence to the "exact" solution with methods ESM and ENSM1, but there is no convergence to that solution for ENSM2. Figures 9, 10 and 11 demonstrate this. Figure 12 shows the difference between the numerical solution and the "exact" solution for the last method. Graphically, it is clear that there is a jump in the initial condition for the velocity and that this is badly estimated by the method; this situation is identical to what happens in the problems of Sections 2 and 3. Furthermore, the rate of convergence of the form $(\Delta t)^e$ for ESM and ENSM1 in q is similar to that observed in the previous sections. Precisely, a log–log fit of the errors gave slope e for the errors in q as 1.0282 and 1.0397 for ESM and ENSM1, respectively. The slopes for the errors in $\dot{q}$ are 0.2706 and 0.2717 for the same methods—slightly lower than the values obtained in previous sections.

Because of the properties of order statistics from large samples, the k_j are asymptotically 1 for large j and hence K_N again has embedded within it a delta-like singularity for large N. Thus we see that, as in the previous section, local damping appears in the limit problem,

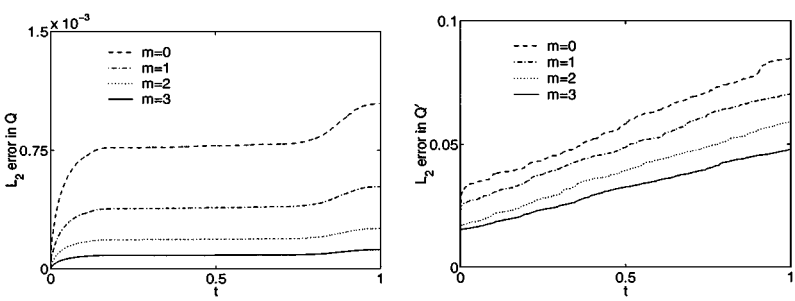

FIG. 10. *L*2-error curves for the position and velocity of the distinguished particle when integrating the linear springs problem with random frequencies with ENSM1.

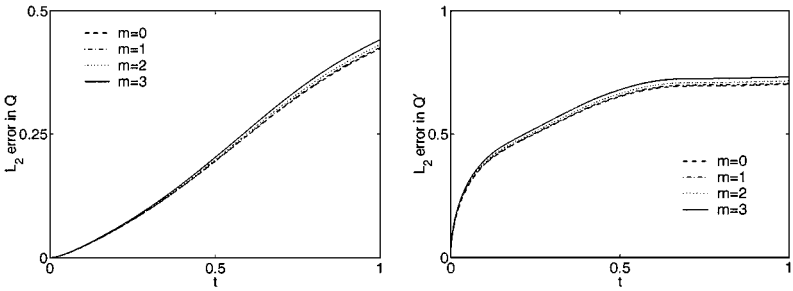

FIG. 11. $L2$-error curves for the position and velocity of the distinguished particle when integrating the linear springs problem with random frequencies with ENSM2.

giving rise to memory kernels whose approximation is delicate. In the next section we consider a problem for which the damping is not local in time.

5. HABIB AND KANDRUP PROBLEM

In this section we consider (1.2) under (1.7), a form of heat bath introduced by Habib and Kandrup [6] with applications in, for example, cosmology. In this case, Hamilton's equations give, with initial conditions (2.2),

$$\begin{aligned} \ddot{q} + V'(q) &= f'(q) \sum_{j=1}^{N} u_j, \quad q(0) = q_0, \quad \dot{q}(0) = p_0, \\ \ddot{u}_j + j^2 u_j &= f(q), \quad u_j(0) = \alpha_j, \quad \dot{u}_j(0) = 0. \end{aligned} \tag{5.1}$$

Solving for u_j in terms of q gives

$$u_j(t) = \alpha_j \cos(jt) + \int_0^t \frac{\sin(j(t-s))}{j} f(q(s))\, ds.$$

Integrating by parts, defining

$$K_N(t) = \sum_{j=1}^{N} \frac{\cos(jt)}{j^2}$$

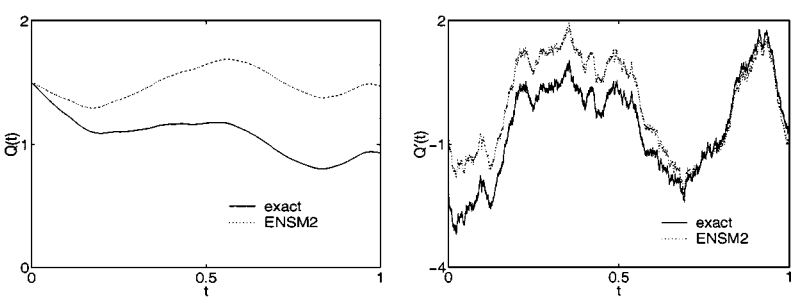

FIG. 12. Position and velocity of the distinguished particle in the linear springs problem with random frequencies when integrated accurately and when integrated with ENSM2.

and

$$Z_N(t) = \sum_{j=1}^{N} \left\{ \alpha_j - \frac{f(q(0))}{j^2} \right\} \cos(jt),$$

we obtain

$$\ddot{q} + V'(q) = f'(q) \left\{ Z_N(t) + K_N(0) f(q(t)) - \int_0^t K_N(t-s) f'(q(s)) \dot{q}(s)\, ds \right\}.$$

Now, by Fourier techniques, the following series converges pointwise and in $L^2((0,\pi))$:

$$\sum_{j=1}^{\infty} \frac{\cos(jt)}{j^2} = \frac{1}{4}t^2 - \frac{\pi}{2}t + \frac{\pi^2}{6} := K_\infty(t).$$

If we choose $\alpha_j = \frac{f(q(0))}{j^2} + \eta_j$ where η_j is $\mathcal{N}(0,1)$ and i.i.d., then almost surely $\int_0^t Z_N(s)ds$ converges uniformly in $(0,\pi)$ to a Brownian bridge $W(t)$. Thus we anticipate that a candidate limit problem for Q is the stochastic integro-differential equation, written formally as

$$\ddot{Q} + f'(Q) \int_0^t K_\infty(t-s) f'(Q(s)) \dot{Q}(s)\, ds + V'(Q) - \frac{\pi^2}{6} f'(Q) f(Q) = f'(Q)\dot{W},$$

$$Q(0) = q_0, \quad \dot{Q}(0) = p_0.$$

Of course, any rigorous interpretation will require a stochastic integral of some form, presumably of Stratonovich type in view of the fact that our approximation to Brownian motion is C^1.

For our numerical experiments, we have considered the particular case $f(z) = z^2/2$. Note that, in contrast with the problems in [12] and in Sections 3 and 4, for this problem there is no jump induced in the initial velocity for the limit problem and the damping is nonlocal in time.

Once again the "exact" solution of (5.1) is found by integrating with N large (16,000) and $N\Delta t$ small ($N\Delta t = 10^{-3}$). Numerical approximations are calculated under (1.3) with $\xi = 1$ and $N = 1{,}000 \times 2^m$, $m = 0, 1, 2, 3$. In this case *all three* methods (1.10), (1.11), and (1.12) appear to converge, although for (1.12) the errors in position q are significantly larger than for (1.10) and (1.11); see Figs. 13, 14, and 15. Convergence is also observed

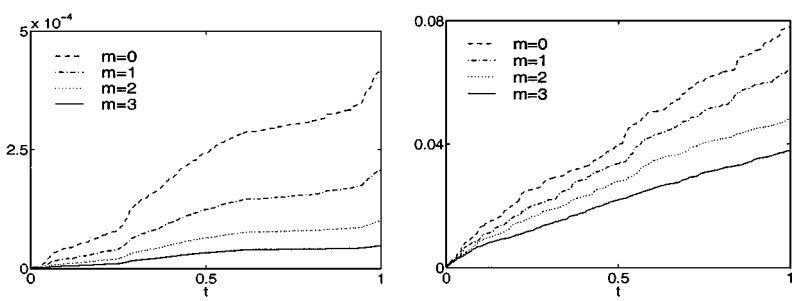

FIG. 13. *L*2-error curves for the position and velocity of the distinguished particle when integrating with ESM.

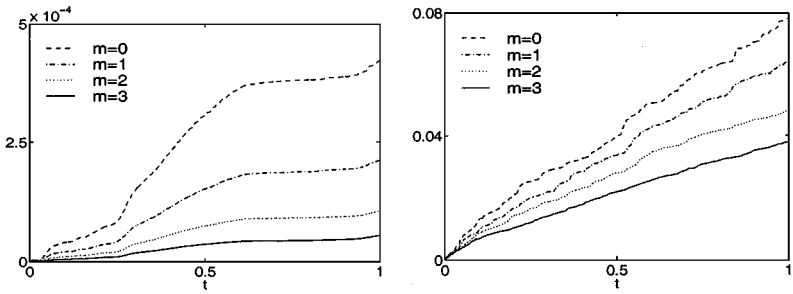

FIG. 14. *L*2-error curves for the position and velocity of the distinguished particle when integrating with ENSM1.

in the $\dot{q}$ variable but in this case (1.12) is as accurate as (1.10) and (1.11). The exponents for the rates of convergence are now 1.0419 for ESM and q, 0.9900 for ENSM1 and q, 0.3266 for ENSM2 and q, 0.3532 for ESM and $\dot{q}$, 0.3532 for ENSM1 and $\dot{q}$, and 0.3823 for ENSM2 and $\dot{q}$.

It is interesting that for this kind of problem, where the limit does not have a jump in the initial condition and where the damping is nonlocal in time, there is no distinction between the three methods (1.10), (1.11), and (1.12) in qualitative terms—all appear to accurately reproduce the macroscopic limit solution when operating in the stiff regime (1.3). The same phenomenon (convergence to the "exact" solution for all three methods) is observed for a variety of other problems in the same class and, in particular, for problems which lead to additive noise and not multiplicative noise. Thus the observations concerning the effect of the smooth memory kernel appear quite robust in relation to changes in the problem specification.

6. RELATION TO MOLECULAR DYNAMICS LITERATURE

In this paper we have studied a class of heat bath models and, in particular, the question of how underresolved simulations of the heat bath affect accuracy of predictions concerning the distinguished particle. The first point to emphasize is that this is a very special class of models and that our investigations can therefore only be regarded as a first step; but we believe that the issue of underresolution, and its relation to prediction of macroscopic quantities, is an important one and that this first step is worth taking. The second point to

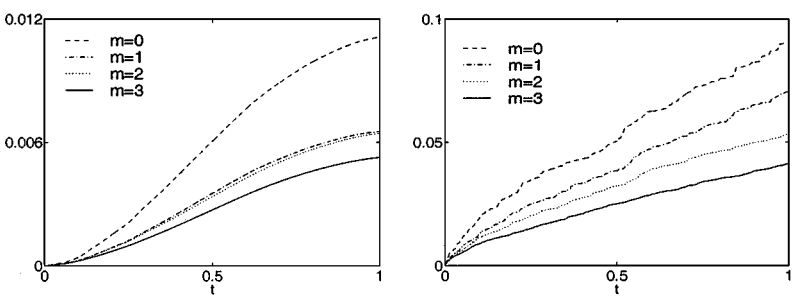

FIG. 15. *L*2-error curves for the position and velocity of the distinguished particle when integrating with ENSM2.

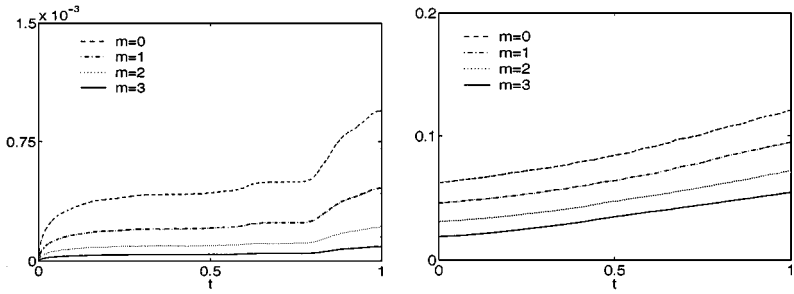

FIG. 16. *L*2-error curves for the position and velocity of the distinguished particle when integrating problem (1.4) with velocity Verlet.

emphasize is that we have confined ourselves to a simple parametrized family of methods, not those used in the molecular dynamics (MD) literature. The third point is that our measures of accuracy do not encompass frequently used diagnostics such as total energy error and the study of physical quantities such as autocorrelation. The final point is that resonances, an issue of some importance in the MD literature, have not been discussed. In this section we address the second, third, and final points in some detail.

6.1. *Other Methods*

The velocity Verlet method (VV) is a symmetric and symplectic second-order method widely used in MD simulations. It may be viewed as a pre- and postprocessed version of the symplectic Euler method ESM studied in previous sections, and it is thus natural to ask whether it inherits the good approximation properties of ESM for the distinguished particle. Figure 16 shows errors for the distinguished particle, when integrating (1.4), with $\xi = 0.1$, using the VV method

$$
\begin{aligned}
P &= p^n + \frac{\Delta t}{2}\left[-V'(|q^n|) + \sum_{j=1}^{N} \frac{\partial F_j}{\partial q}\left(U_j^n, q^n\right)\right],\\
Q_j &= V_j^n - \frac{\Delta t}{2}\frac{\partial F_j}{\partial q}\left(U_j^n, q^n\right),\\
q^{n+1} &= q^n + \Delta t\, P,\\
U_j^{n+1} &= U_j^n + \Delta t\, Q_j,\\
p^{n+1} &= P + \frac{\Delta t}{2}\left[-V'(|q^{n+1}|) + \sum_{j=1}^{N} \frac{\partial F_j}{\partial q}\left(U_j^{n+1}, q^{n+1}\right)\right],\\
V_j^{n+1} &= Q_j - \frac{\Delta t}{2}\frac{\partial F_j}{\partial q}\left(U_j^{n+1}, q^{n+1}\right).
\end{aligned}
$$

Figure 16 should be compared with Fig. 2 which shows nearly identical behaviour for the ESM. Indeed fits to the slopes of the error for VV and ESM differ by only (approximately) 0.5% for the position and 2% for the velocity.

This experiment is interesting because it shows that, although VV is formally second-order accurate and ESM only first-order accurate, when predicting the motion of the

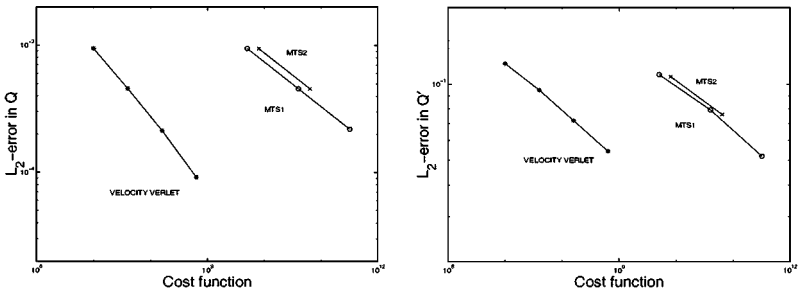

FIG. 17. $L2$-error for the position and velocity of the distinguished particle after time 1 against computational cost when integrating problem (1.4) with velocity Verlet (*, $N = 1000, 2000, 4000, 8000$), MTS1 (o, $N = 1000, 2000, 4000$), and MTS2 (x, $N = 1000, 2000$).

distinguished particle in an underresolved heat bath, the methods are equally accurate. There are two reasons for this: (i) the distinguished particle has highly irregular acceleration (the limit problem is likely to be an SDE for which the acceleration does not exist as a bounded function) and this limits accuracy; (ii) the truncation for the limit problem to a finite N is a dominant error.

We have also studied multiple time-scale methods [5, 13, 14]. These are widely used in the MD literature, in particular in the reversible versions described in [13, 14]. The first, MTS1, is based on ideas in [13]. It is constructed as follows: we consider as fast and slow forces the respective terms

$$F_f = \sum_{j=N/2+1}^{N} \frac{\partial F_j}{\partial q}(u_j, q), \quad F_s = \sum_{j=1}^{N/2} \frac{\partial F_j}{\partial q}(u_j, q) - V'(|q^n|)\frac{q_n}{|q_n|}.$$

The method is based on velocity Verlet in the following way. A step $\Delta t = \xi/N$ of the integration consists of

- advancing the velocities $\Delta t/2$ units of time with the explicit symplectic Euler method (ESM) taking into account only the slow forces;
- advancing the velocities and positions Δt units of time from the previous values, using N steps of stepsize $\delta t = \Delta t/N$ of the velocity Verlet method and taking into account only the fast forces;
- advancing the velocities $\Delta t/2$ units of time from the previous values, using explicit Euler and taking into account only the slow forces.

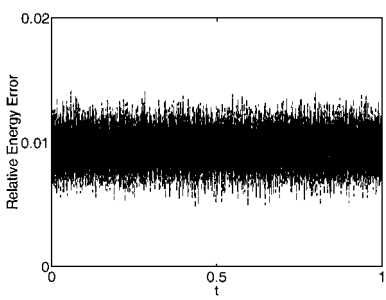

FIG. 18. Relative energy error in the whole system when integrating with ESM and $N = 8000$, $N\Delta t = 0.1$.

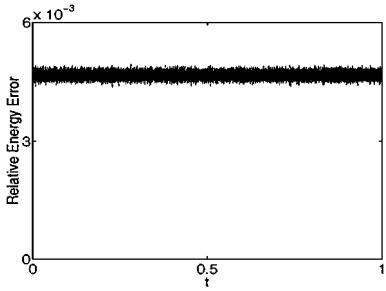

FIG. 19. Relative energy error in the whole system when integrating with velocity verlet and $N = 8000$, $N\Delta t = 0.1$.

Note that with this method the high-oscillatory springs are integrated much more accurately than they are in the methods applied in previous sections and than they are in VV. An important question is whether the cost of this greater accuracy is justified.

The second multiple time-scale method, MTS2, is based on ideas in [14] and is constructed as follows. It consists of an embedded factorization of the propagator of the method, similar to the one given previously, but more complicated, integrating several groups of different frequencies with different time-steps. More precisely, we have considered the following:

- stepsize dt1 $= 10^3\Delta t/N$ for the frequencies 1 to $N/500$;
- stepsize dt2 $=$ dt1$/10$ for the frequencies $N/500 + 1$ to $N/50$;
- stepsize dt3 $=$ dt2$/10$ for the frequencies $N/50 + 1$ to $N/5$;
- stepsize dt4 $=$ dt3$/10$ for the frequencies $N/5 + 1$ to N.

For MTS1, the number of times the function $\frac{\partial F_j}{\partial_q}$ must be evaluated to integrate to time 1 is approximately $0.5(1 + N)N^2/\xi$, compared with N^2/ξ required for single velocity Verlet with $N\Delta t = \xi$. For MTS2, the number of evaluations is approximately

$$\frac{N^3}{\xi}\left[\frac{4}{5} + \frac{9}{500} + \frac{9}{50{,}000} + \frac{1}{5 \times 10^5}\right] \approx \frac{4N^3}{5\xi}.$$

However, both the MTS methods are, of course, considerably more accurate when considered as approximations to the whole system. It is hence of interest to compare accuracy per unit cost for the MTS methods and VV. We do this, focusing interest only on the error in computing the distinguished particle. What we find is that the cost per unit error of

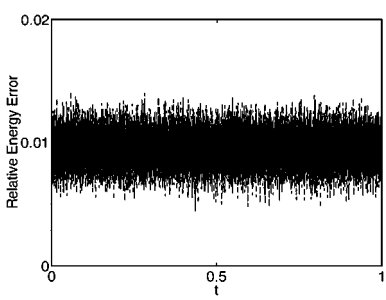

FIG. 20. Relative energy error for the whole system when integrating with ENSM2 and $N = 8000$, $N\Delta t = 0.1$.

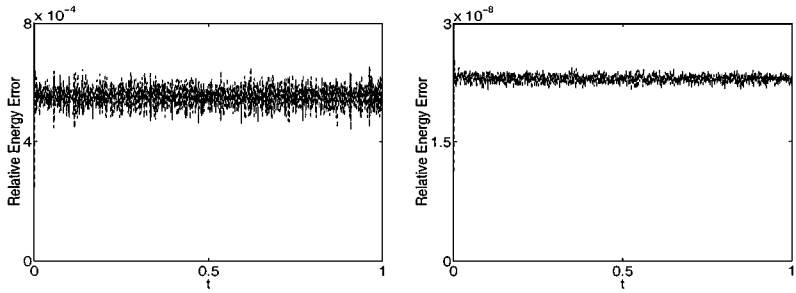

FIG. 21. Relative energy error for the whole system when integrating Problem (1.4) with MTS1 (left) and MTS2 (right), $N = 1000$ and $N\Delta t = 0.1$.

the VV method is considerably smaller than for both our implementations of the MTS method. Figure 17, which is based on experiments with problem (1.4), illustrates this phenomenon. Of course it is *possible* that, by optimizing the splittings in the MTS algorithms, a competitive MTS method could be found. But the experiments suggest quite strongly that, if only errors in macroscopic quantities are of interest, then some care needs to be taken in determining how to evaluate the relative merits of various schemes; for our particular model problems the straightforward VV implementation appears to be superior to MTS.

6.2. *Other Error Indicators*

(i) Total energy. The total energy is a commonly used diagnostic in the MD literature. Figures 18, 19, 20, and 21 show the relative energy error for simulations of (1.4); all are performed in the regime $N = 8000$ and $N\Delta t = 0.1$ with the exception of the MTS methods which are integrated at $N = 1000$. Except for MTS2, increasing N does not cause the relative energy error to go to zero; it remains approximately the same size. The relative accuracy of the methods, considered as approximations for the whole systems and not just the distinguished particle, is manifest in these figures and shows that the total energy error is a useful diagnostic in that sense. Note, however, that the ENSM2 method does not correctly predict the distinguished particle motion, but this fact is *not* manifest in the energy error—Figs. 18 and 20 are quantitatively very similar. Note also that while the VV has a much smaller energy error than the ESM, at the particle level this accuracy advantage disappears. In summary, energy error is quite misleading when evaluating the accuracy and efficiency of underresolved methods for macroscopic quantities.

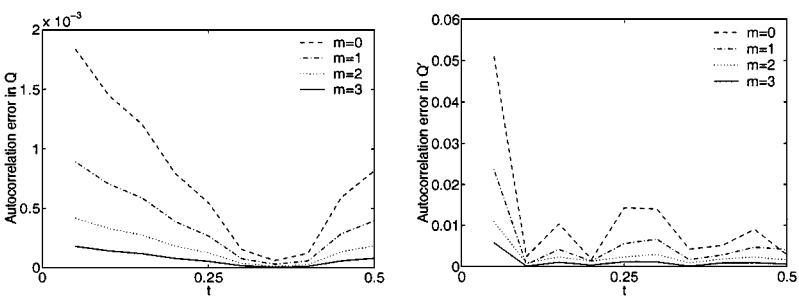

FIG. 22. Autocorrelation error in position and velocity when integrating problem (1.4) with ESM and $N\Delta t = 0.1$.

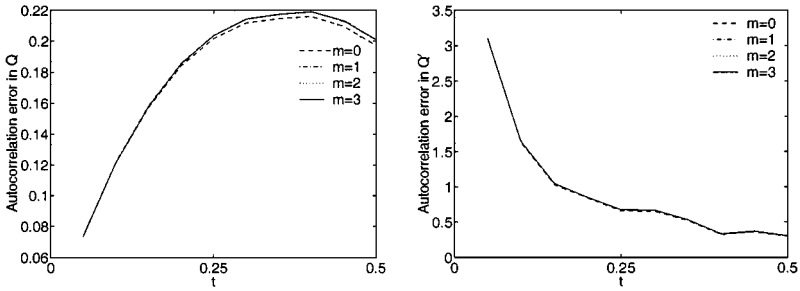

FIG. 23. Autocorrelation error in position and velocity when integrating problem (1.4) with ENSM2 and $N\Delta t = 0.1$.

(ii) Autocorrelation. In earlier sections we have chosen to monitor the particle position and velocity errors in the L_2 norm in time because that norm is appropriate for the analysis which has been performed in some cases [1, 12]. Note, however, that the definition of this norm means that all errors are monotone increasing; this does not imply that pointwise velocity errors are increasing. To emphasize this fact we look at L_∞ errors in the particle position and velocity autocorrelation functions

$$C_q(t) = \frac{1}{t}\int_0^t q(s)q(s+t)\,ds, \quad C_p(t) = \frac{1}{t}\int_0^t p(s)p(s+t)\,ds,$$

for the ESM method and the ENSM2 method applied to problem (1.4). Figure 22 shows convergence of these quantities for the ESM method, while Fig. 23 illustrates nonconvergence for the ENSM2 method. These graphs simply represent what we have seen already in Section 3, here visualized in terms of physically meaningful quantities.

6.3. *Resonances*

Resonances impose significant limitations on explicit integrators in MD simulations [11] and it is therefore of interest to understand their role in our context. We have seen no evidence of resonance effects in our simulations. There are two likely explanations for this: our time-step restriction (1.3) is sufficient to avoid them for the most part; even if they do occur they are limited to infrequent effects which, in any case, occur in the high frequency modes whose accuracy does not concern us directly.

In fact, we have calculated the frequency power spectrum for the position and velocity of the distinguished particle corresponding to problem (1.4). We have considered the "exact"

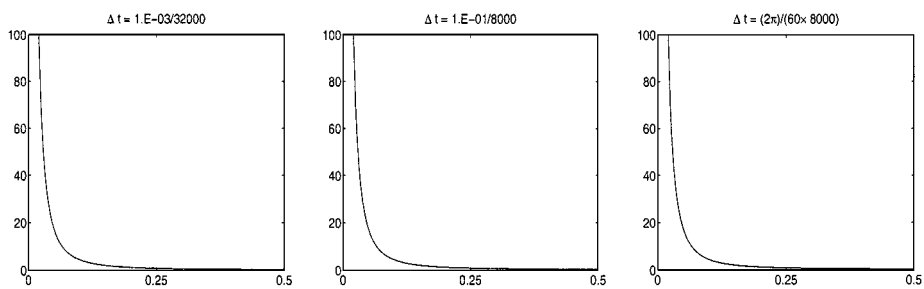

FIG. 24. Frequency power spectrum for the position of the distinguished particle when integrating problem (1.4) "exactly" and with VV, $N = 8000$ and various values of $N\Delta t$.

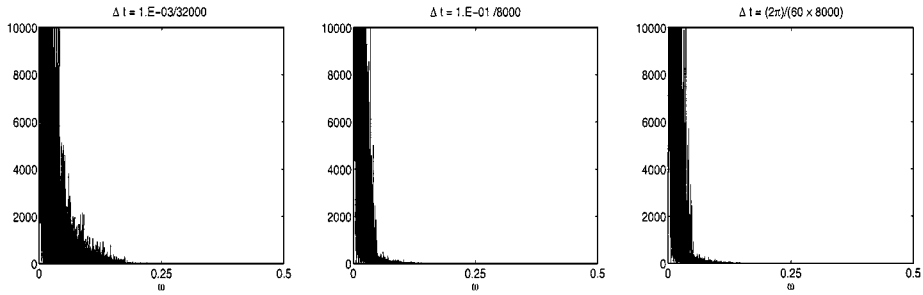

FIG. 25. Frequency power spectrum for the velocity of the distinguished particle when integrating problem (1.4) "exactly" and with VV, $N = 8000$ and various values of $N\Delta t$.

solution determined in Section 2, as well as the numerical approximation given by velocity Verlet for several values of $N\Delta t$ (just small enough to give stability). We have not seen any evidence of resonant behaviour. In Figs. 24 and 25, we consider $N = 8{,}000$ and then $N\Delta t = 0.1$ and $N\Delta t = 2\pi/60$. The power spectrum is calculated through fast Fourier transform. For the "exact" solution and the first numerical approximation we apply it to 80,000 uniform values in time [0, 1]. For the second numerical approximation, we consider the 76,394 values given in the same interval. Notice that we have normalized the frequency to vary from 0 to 1 although we have just drawn half the spectrum because of the symmetry due to the real input for the FFT. For the position, we have limited the power spectrum to $[0, 10^2]$, in order to provide a clear comparison with the "exact" case. We have fit the spectral data to a function of the form C/ω^α, getting in all cases $C = 0.08075\ldots, \alpha = 1.8045\ldots$. (The results for each integration differ only in the decimal places which are not shown.) As for the velocity, we have limited the spectrum to $[1, 10^4]$. In Fig. 25, we can see that the "exact" solution has a heavier weight in some of the frequencies than the approximations calculated with $N = 8{,}000$. This is natural if we take into account that the "exact" solution was calculated with $N = 32{,}000$ and therefore more frequencies arise there. (In fact, we are interested in the limit when N grows to infinity.) In any case, the numerical approximations do not show any significant frequency which is not present in the "exact" solution. In summary, we see no evidence of resonance.

7. CONCLUSIONS

The results in Sections 2, 3, and 4 are qualitatively different from those in Section 5. In Section 5 all methods appear to reproduce the macroscopic limit; in the other sections only certain methods reproduce the correct limit. It is our belief that the key difference which gives rise to this observation is the nature of the memory kernel K_N. In Sections 3 and 4 this kernel has embedded within it delta-like behaviour, for $N \gg 1$, leading to local-in-time damping; in Section 5 the kernel is smooth as $N \to \infty$ and the damping is hence nonlocal in time. (In Section 2 we cannot compute an explicit damping kernel, because of the nonlinear nature of the coupling, but in the linear spring analogue of the problem, which is considered in [12], the kernel again contains a delta-like singularity.)

Thus the approximation of Fourier representations of delta functions, by numerically generated oscillators, appears key regarding the underresolved simulations of (1.8). Analysis of this issue is pursued in detail in [1].

Looking at the subject more broadly, the experiments in this paper indicate that it is possible to accurately compute macroscopic quantities in mechanical heat baths without detailed resolution of fast scales in the heat bath, and therefore without having to resort to multiple time-scale methods. By considering a wide variety of problems we have considerably extended the range of heat bath models which allow this conclusion to be drawn. This in turn suggests that pursuing this question for other problems in the general form (1.1) is a worthwhile endeavour. In particular, the study of Hamiltonian problems with a more applied flavour, such as those arising in molecular dynamics, would be natural. Our studies in Section 6 touch on some of the issues that arise in this context.

REFERENCES

1. B. Cano, A. M. Stuart, E. Süli, and J. O. Warren, Stiff oscillatory systems, delta jumps, and white noise, *Found. Comput. Math.*, to appear.
2. A. J. Chorin, A. Kast, and R. Kupferman, Underresolved computation and optimal predictions, *Comm. Pure Appl. Math.* **10**, 1231 (1999).
3. A. J. Chorin, A. Kast, and R. Kupferman, Optimal prediction of underresolved dynamics, *Proc. Natl. Acad. Sci.* **95**, 4094 (1998).
4. G. W. Ford and M. Kac, On the quantum Langevin equation, *J. Stat. Phys.* **46**, 803 (1987).
5. B. García-Archilla, J. M. Sanz-Serna, and R. D. Skeel, Long-time-step methods for oscillatory differential equations, *SIAM J. Sci. Comput.* **20**, 930 (1998).
6. S. Habib and H. E. Kandrup, Nonlinear noise in cosmology, *Phys. Rev. D* **46**, n. 12, 5303 (1992).
7. O. H. Hald, Optimal prediction and the Klein–Gordon equation, *Proc. Natl. Acad. Sci.* **96**, 4774 (1999).
8. J. P. Kahane, *Some Random Series of Functions*, 2*nd* ed., (Cambridge Univ. Press, Cambridge, UK, 1985).
9. A. Kast, Optimal prediction of stiff oscillatory mechanics, *Proc. Natl. Acad. Sci.* **97**, 6253 (2000).
10. R. D. Richtmyer and K. W. Morton, *Difference Methods for Initial Value Problems*, (Wiley, New York, 1967).
11. T. Schlick, M. Mandziuk, R. D. Skeel, and K. Srinivas, Nonlinear resonance artifacts in molecular dynamics *simulations*, *J. Comput. Phys.* **140**, 1 (1998).
12. A. M. Stuart and J. O. Warren, Analysis and experiments for a computational model of a heat bath, *J. Stat. Phys.* **97**, 687 (1999).
13. M. Tuckerman, B. J. Berne, and G. J. Martyna, Reversible multiple time scale molecular dynamics, *J. Chem. Phys.* **97** (3), 1990 (1992).
14. M. E. Tuckerman and M. Parrinello, Integrating the Car–Parrinello equations. II. Multiple time scale techniques, *J. Chem. Phys.* **101** (2), 1316 (1994).
15. R. Zwanzig, Nonlinear generalized Langevin equations, *J. Stat. Phys.* **9**, 215 (1973).